Understanding Atomoxetine Exposure Variability in Children and Adolescents With ADHD Through Population Pharmacokinetics

The Journal of Clinical Pharmacology
2026, 66(4) e70168

DOI: 10.1002/jcph.70168

Kevin. V. Tobin, PhD[1], Addison Pritchett, MS[2], J. Steven Leeder, PharmD, PhD[2], Joga Gobburu, PhD[1], and Allison Dunn, PharmD[1]

Abstract

Atomoxetine, a selective norepinephrine reuptake inhibitor, is a nonstimulant alternative to treat attention-deficit/hyperactivity disorder in children and adolescents. Atomoxetine exposure is highly variable due to cytochrome P450 polymorphism; however, the impact of these genetic variations has not been adequately characterized in the pediatric population. A population pharmacokinetic (PK) model was developed to evaluate steady-state atomoxetine exposures after oral administration in a large, heterogeneous population of children and adolescents with different metabolic phenotypes. Due to the highly variable and complex absorption between subjects and occasions, a two-stage approach was implemented, treating each participant/occasion as a separate individual. First, the individual atomoxetine parameters were estimated using a one-compartment distribution model with zero-order duration into a depot compartment followed by first-order absorption into the central compartment with linear elimination. Next, population-level parameters were obtained, and covariate analysis was performed. Using actual body weight, relative bioavailability based on CYP2D6 or CYP2C19 phenotype, and CYP2D6 clearance effects in the model reduced the variability from 81.6% to 64.5% and 92.4% to 75.5% for apparent volume and apparent clearance, respectively. The final model showed adequate precision in PK parameters and accuracy in exposure metrics. Following prospective validation, this model could be used to provide clinicians with individualized dosing targets when prescribing atomoxetine to children and adolescents based on their genetic disposition.

Keywords

ADHD, atomoxetine, CYP2C19, CYP2D6, pediatrics, population pharmacokinetics

Introduction

Atomoxetine is a selective norepinephrine reuptake inhibitor (SNRI) indicated for the treatment of attention-deficit/hyperactivity disorder (ADHD) in children, adolescents, and adults.[1] Atomoxetine is a non-stimulant alternative to ADHD treatment with amphetamine- and methylphenidate-related formulations, providing a lower side-effect profile that could be beneficial to children and adolescents.

Following oral administration and absorption, atomoxetine is primarily biotransformed in the liver by cytochrome P450 2D6 (CYP2D6) and to a lesser extent by cytochrome P450 2C19 (CYP2C19).[2] Single-dose atomoxetine pharmacokinetics in children and adolescents with varying CYP activities have been studied previously,[3,4] but not at daily-dosing, steady-state concentrations. On average, atomoxetine exposures were consistently found to be >10-fold higher in poor metabolizers (PMs) compared to normal metabolizers (NMs) when administered the same weight-based dose. Previous studies on atomoxetine pharmacodynamics suggest that approximately 40% of the ADHD patients are non-responders regardless of atomoxetine exposure.[5] Despite atomoxetine being a viable alternative to stimulants for treating ADHD in children and adolescents, atomoxetine prescription rates in this group have been on a steady decline.[6] The perception that atomoxetine is not effective could be a consequence of inadequate therapeutic exposure for a significant time early on in treatment, clinical response being delayed until after completion of clinical follow-up

[1]Center for Translational Medicine, University of Maryland School of Pharmacy, Baltimore, MD, USA
[2]Department of Pediatrics, Children's Mercy Research Institute, Kansas City, MO, USA

Submitted for publication 29 July 2025; accepted 5 February 2026.

Corresponding Author:
Allison Dunn, PharmD, 20 N Pine St., School of Pharmacy, Room S523, Baltimore, MD 21201
Email: adunn@rx.umaryland.edu

(>9 weeks), or patients being inherently non-responsive due to pharmacodynamic factors.[7]

Despite the polymorphic nature of CYP2D6 and CYP2C19 activities causing highly variable systemic exposure of atomoxetine following oral administration, the atomoxetine product label[8] recommends a weight-based starting dose of 0.5 mg/kg/day in all children <70 kg regardless of CYP2D6 or CYP2C19 activity status. Ignoring the CYP enzyme activities for the initial dosing can cause more adverse events in PMs (including increased heart rate and/or increased blood pressure[8]) and could reduce the likelihood of adequate therapeutic drug exposure in normal metabolizers.[9,10] The purpose of this study is to evaluate steady-state atomoxetine exposures in a large heterogeneous population of children and adolescents with different predicted metabolic phenotypes and develop a robust model that can be utilized clinically to minimize the risk of inadequate exposure and potential therapeutic failure in patients with ADHD who may benefit from the drug.

Methods

Study Populations

Demographic and pharmacokinetic (PK) data were combined from three separate studies[3,11] in which atomoxetine was administered to children and adolescents with a confirmed diagnosis of ADHD and who had undergone genotype analysis for *CYP2D6* and *CYP2C19*. All studies were approved by the Institutional Review Board at Children's Mercy Kansas City. Written informed consent was obtained from each participant prior to enrollment. Combined, these studies consisted of 86 participants ranging from 6 to 17 years of age.

Genotyping and Phenotyping

Detailed procedures for genotyping were previously described.[3,12] Briefly, participant-specific phenotypes were determined based on each participant's genotype call by assigning an activity score based on CYP diplotype using updated standardized guidelines published by the Clinical Pharmacogenetic Implementation Consortium (CPIC). Predicted phenotype classification was assigned to each study participant according to these guidelines as follows: ultra-rapid metabolizers (UMs) as having an activity score >2, NMs as having an activity score 1-s2, intermediate metabolizers (IMs) as having an activity score of 0.25-1, and PMs as having an activity score of 0.[13]

Dosing and Study Design

Three study datasets were combined for this analysis; they are presented in the supplemental materials (Table S1) and described below. The first study, herein referred to as "Study A," involved a single oral weight-based dose of 0.5 mg/kg regardless of CYP2D6 phenotype, as suggested in the product label.[8] Plasma concentrations of atomoxetine were measured up to 72 h post-dose for PMs, up to 24 h for IMs and NMs, and 12 h for UMs. Details of the study design and results were first reported by Brown et al,[3] and a more comprehensive analysis of parent and metabolite kinetics from the same study participants has been described by Cheng et al.[4] The second study herein referred to as "Study B" involved a single atomoxetine oral dose to validate an unpublished model built using the data from Study A, intended for use in an exposure escalation study to individualize atomoxetine dosing to achieve a target maximum plasma concentration of 400 ng/mL based on CYP2D6 phenotype. To assess inter-occasion variability, each participant was invited to return for a second study visit to assess day-to-day variability in atomoxetine disposition; the time interval between study days ranged from 15 to 386 (mean, 164 days). The study protocol was identical for both study days, with samples collected over 12 h for NMs or UMs and up to 72 h for IMs. The third study herein, referred to as "Study C," represents pharmacokinetic data following the first dose of atomoxetine and up to two subsequent study days at steady state for the exposure-escalation study alluded to above (grant P50HD090258, "GOLDILOKs: Genomic- and Ontogeny-Linked Dose Individualization and cLinical Optimization for Kids"; ClinicalTrials.gov registration # NCT03154359). For each study participant, atomoxetine dosing was individualized using the unpublished model referred to earlier to achieve a target plasma concentration (C_{max}) of 400 ng/mL at steady-state. Serial atomoxetine plasma concentrations were measured after the single dose up to 12 h for UMs or NMs and up to 72 h for IMs and PMs. After the single-dose PK session (up to 72 h) was concluded, participants were instructed to take a consistent oral atomoxetine dose daily (twice daily dosing for two participants), and two steady-state PK sessions were conducted at weeks 6 ± 2 and 18 ± 2 weeks (with documented adherence for at least 2 weeks prior to the steady-state PK session); plasma concentrations were measured up to 12 h for UMs or NMs and up to 24 h for IMs and PMs. All participants were instructed to fast from midnight to 2 h after dosing (only water permitted), after which an age-appropriate diet was resumed.

Data Analysis

Non-compartmental analysis (NCA) was performed on observed data to compare C_{max}, t_{max}, $AUC_{0\text{-}24h}$, and half-life across different CYP2D6 phenotypes and dosing scenarios. Data preparation, statistical analysis, and visualization of the data and output were performed using R 4.2.3 (R Core Team, Vienna, Austria). Nonlinear mixed effects modeling was used to characterize

atomoxetine plasma concentrations. Due to the inconsistent absorption between subjects and occasions, separate occasions of atomoxetine administration (i.e., repeated single doses or single doses and steady-state occasions in the same subject) were treated as separate individuals. The population PK model was built using a two-stage approach. First, a base structural model with residual unexplained variability (RUV) was developed on individual PK profiles to obtain individual parameters. Then, the population level parameters, typical values, and between-subject variability (BSV) were estimated for covariate exploration to explain the BSV. Modeling was performed using Pumas v2.5.1 (Pumas AI, Baltimore, MD, USA).

Population Pharmacokinetic Modeling

Structural Model Development. Based on the observed atomoxetine plasma concentrations showing a single linear elimination phase, a single-compartment model with first-order elimination was used. Multiple absorption models were evaluated and selected based on a decrease in the objective value function and goodness of fit. Individual parameters were estimated for single or parallel absorption using first-order and/or delayed (zero-order input into a depot followed by first-order absorption to the central compartment) pathways. These structural models involved parameters including fraction of drug to each absorption pathway, duration of zero-order absorption, first-order absorption rate constants, apparent central volume (Vc/F), and apparent clearance (CL/F).

Additive, proportional, and combined residual error models were evaluated to account for the RUV between observations and model predictions. The combined error model is described as

$$\mathrm{OBS}_{i,j} = \mathrm{PRED}_{i,j} + \mathrm{PRED}_{i,j} \cdot \varepsilon_{\mathrm{prop},i,j} + \varepsilon_{\mathrm{add},i,j} \quad (1)$$

where $\mathrm{OBS}_{i,j}$ and $\mathrm{PRED}_{i,j}$ are the observation and prediction for the i-th participant at time j, respectively, and $\varepsilon_{\mathrm{prop},i,j}$ and $\varepsilon_{\mathrm{add},i,j}$ are the proportional and additive participant-time-specific observation deviations from the predictions that follow a normal distribution with a mean of zero and a variance of σ^2_{prop} or σ^2_{add}, respectively.

BSV was assumed to be log-normally distributed as

$$\theta_i = \theta_{tv} \cdot e^{\eta_{\theta,i}} \quad (2)$$

where θ_i is the individual parameter, θ_{tv} is the typical population parameter, and $\eta_{\theta,i}$ is the participant-specific deviation from the population typical parameter that follows a normal distribution with a mean of zero and a variance of ω^2_θ for parameter θ. Typical participant values and variance for all PK parameters were estimated as the mean and variance of the normally distributed individual parameters.

Covariate Model Development. After the structural model was selected, participant-specific covariates were analyzed to explain variability in PK parameters. Potential covariates were assessed by exploring the distribution of $\eta_{\theta,i}$ stratified by different subpopulations (empirical Bayes estimates [EBEs]). Covariates were added sequentially if they were physiologically meaningful and supported the explanation of the variability in the PK parameters, as noted by reduction or removal of trends in the EBEs, decrease in the objective value function, and reduction in parameter BSV. Body weight was included in the model using allometric scaling as

$$\theta_i = \theta_{tv} \cdot \left(\frac{\mathrm{wt}_i}{70}\right)^{b_\theta} \cdot e^{\eta_{\theta,i}} \quad (3)$$

where wt_i is the individual weight, 70 is the typical adult body weight in kg, and b_θ is the allometric scaling exponent for parameter θ, which was 1.0 when applied to volume and 0.75 when applied to clearance. The effect of relative bioavailability on apparent volume (based on CYP phenotype) was explored in the model as

$$\mathrm{Vc/F}_i = \mathrm{Vc/F}_{tv} \cdot \left(\frac{\mathrm{wt}_i}{70}\right)^{1.0} \cdot \left(\frac{1}{F_{rel}}\right) \cdot e^{\eta_{\mathrm{Vc/F},i}} \quad (4)$$

where F_{rel} is the relative bioavailability compared to NMs ($F_{rel,NM} = 1$). The same relative bioavailability (based on phenotype), along with a relative effect of CYP2D6 phenotype on clearance, was explored as

$$\mathrm{CL/F}_i = \mathrm{CL/F}_{tv} \cdot \left(\frac{\mathrm{wt}_i}{10}\right)^{0.75} \cdot \left(\frac{1}{F_{rel}}\right) \cdot (1 + E_{\mathrm{CYP2D6}}) \cdot e^{\eta_{\mathrm{CL/F},i}} \quad (5)$$

where E_{CYP2D6} is the relative effect of CYP2D6 enzyme activity on clearance compared to CYP2D6 NMs ($E_{\mathrm{CYP2D6,\ NM}} = 0$). Additionally, the effect of CYP2C19 enzyme activity on clearance compared to CYP2C19 NMs was explored similarly to Equation (5).

Model Qualification. Precision of the final covariate model parameter estimates was assessed using nonparametric bootstrap simulations. The final model was fitted to 200 datasets that were sampled with replacement from the original dataset (without CYP2D6 stratification) to obtain the mean and 95% confidence interval of the parameter estimates. The accuracy of the final covariate model was assessed by performing simulations using 1000 datasets generated by resampling (with replacement) individuals (retaining all EBEs for each individual) from each CYP2D6 phenotype

Table 1. Summary Statistics of Participant Demographics Included in this Analysis Stratified by CYP2D6 Enzyme Activity Phenotype.

		CYP2D6 Phenotype			
Characteristic	Overall N = 86	Intermediate N = 41	Normal N = 35	Poor N = 6	Ultra Rapid N = 4
Age (years), Mean (SD)	12.6 (3.2)	12.5 (3.3)	12.3 (3.1)	13.7 (3.4)	13.7 (3.3)
Weight (kg), Mean (SD)	54.5 (26.4)	57.2 (29.5)	50.2 (22.1)	61.2 (26.3)	54.2 (30.9)
Height (cm), Mean (SD)	153.9 (19.3)	155.2 (20.9)	151.6 (18.1)	158.8 (18.6)	152.8 (17.0)
Body-Mass Index, Mean (SD)	21.8 (6.4)	22.2 (6.7)	20.9 (5.9)	23.2 (5.7)	22.5 (10.7)
Obese, n (%)	22 (26%)	10 (24%)	9 (26%)	2 (33%)	1 (25%)
Heart Rate (BPM), Mean (SD)	74.0 (15.6)	73.8 (15.9)	75.4 (16.6)	69.3 (7.5)	69.5 (15.1)
Systolic BP (mmHg), Mean (SD)	113.0 (11.2)	114.1 (11.5)	113.4 (11.4)	107.2 (7.9)	106.3 (9.0)
Diastolic BP (mmHg), Mean (SD)	64.2 (8.4)	65.3 (9.2)	63.5 (8.1)	60.5 (2.9)	64.8 (8.3)
Race, N (%)					
Asian	1 (1.2%)	1 (2.4%)	0 (0%)	0 (0%)	0 (0%)
Black	28 (33%)	11 (27%)	12 (34%)	2 (33%)	3 (75%)
Hispanic/Latino	1 (1.2%)	0 (0%)	1 (2.9%)	0 (0%)	0 (0%)
Mixed race	11 (13%)	4 (9.8%)	7 (20%)	0 (0%)	0 (0%)
Native Hawaiian/Pacific Islander	1 (1.2%)	1 (2.4%)	0 (0%)	0 (0%)	0 (0%)
White	44 (51%)	24 (59%)	15 (43%)	4 (67%)	1 (25%)
Sex, N (%)					
Female	16 (19%)	8 (20%)	7 (20%)	0 (0%)	1 (25%)
Male	70 (81%)	33 (80%)	28 (80%)	6 (100%)	3 (75%)
CYP2C19 Activity, N (%)					
Intermediate	21 (24%)	7 (17%)	12 (34%)	0 (0%)	2 (50%)
Normal	31 (36%)	14 (34%)	13 (37%)	3 (50%)	1 (25%)
Poor	2 (2.3%)	2 (4.9%)	0 (0%)	0 (0%)	0 (0%)
Rapid	26 (30%)	13 (32%)	10 (29%)	2 (33%)	1 (25%)
Ultra Rapid	6 (7.0%)	5 (12%)	0 (0%)	1 (17%)	0 (0%)

SD: standard deviation; N: count; BP: blood pressure. Obesity was defined as a body-mass index at or above the 95th percentile based on standard growth chart criteria.

and dosing scenario (single dose or steady-state dosing) to match the original dataset. Individual etas were calculated for each participant using Equations (2), (4), and (5). For these simulations, the typical parameter estimates from the final covariate were fixed. Visual predictive checks (VPCs) were performed on simulated atomoxetine plasma concentrations, where the 10th, 50th, and 90th percentiles of the predicted plasma concentration over time with 95% visual prediction interval of each percentile were compared to the corresponding percentiles of the observed data for each applicable CYP2D6 phenotype at each steady-state session. Additionally, quantitative predictive checks (QPCs) were performed on important PK parameters (C_{max} and $AUC_{0\text{-}24h}$) derived using NCA on the simulated PK profiles. For the QPC, the 5th, 50th, and 95th percentiles of the predicted C_{max} were compared to the median observed C_{max} for each applicable CYP2D6 phenotype at each steady-state session. The prediction error was calculated as

$$\%PE = 100 \cdot \frac{PRED - OBS}{OBS} \quad (6)$$

where PRED is the predicted median C_{max} or $AUC_{0\text{-}24h}$ in each of the 1000 simulated datasets and OBS is the observed median C_{max} or $AUC_{0\text{-}24h}$. The 95% confidence interval around the median prediction error was calculated for IMs and NMs at single dose and steady-state dosing.

Results

Data

Participant demographics and baseline characteristics are summarized in Table 1. A total of 86 participants were analyzed (33 participants had one single dose visit, 21 participants had two single dose visits, 12 participants had one single dose and one steady state visit, and 20 participants had one single dose and two steady state visits; 159 total visits) with an age of 12.6 ± 3.2 years, a weight of 54.5 ± 26.4 kg, and a body-mass index of 21.8 ± 6.4. Despite the large difference in the number of participants between the four CYP2D6 phenotypes (6 PMs, 41 IMs, 35 NMs, and 4 UMs), age, weight, height, body–mass index, obesity, heart rate, and blood pressure were evenly distributed across the four CYP2D6 phenotypes. The majority of participants were reported to be White (51%), with the next largest group reported as Black (33%). A majority of the CYP2D6 PMs and IMs were reported White, while a majority of the UMs were reported as Black. There was a larger proportion of male participants (81%), and all 6 PMs were male.

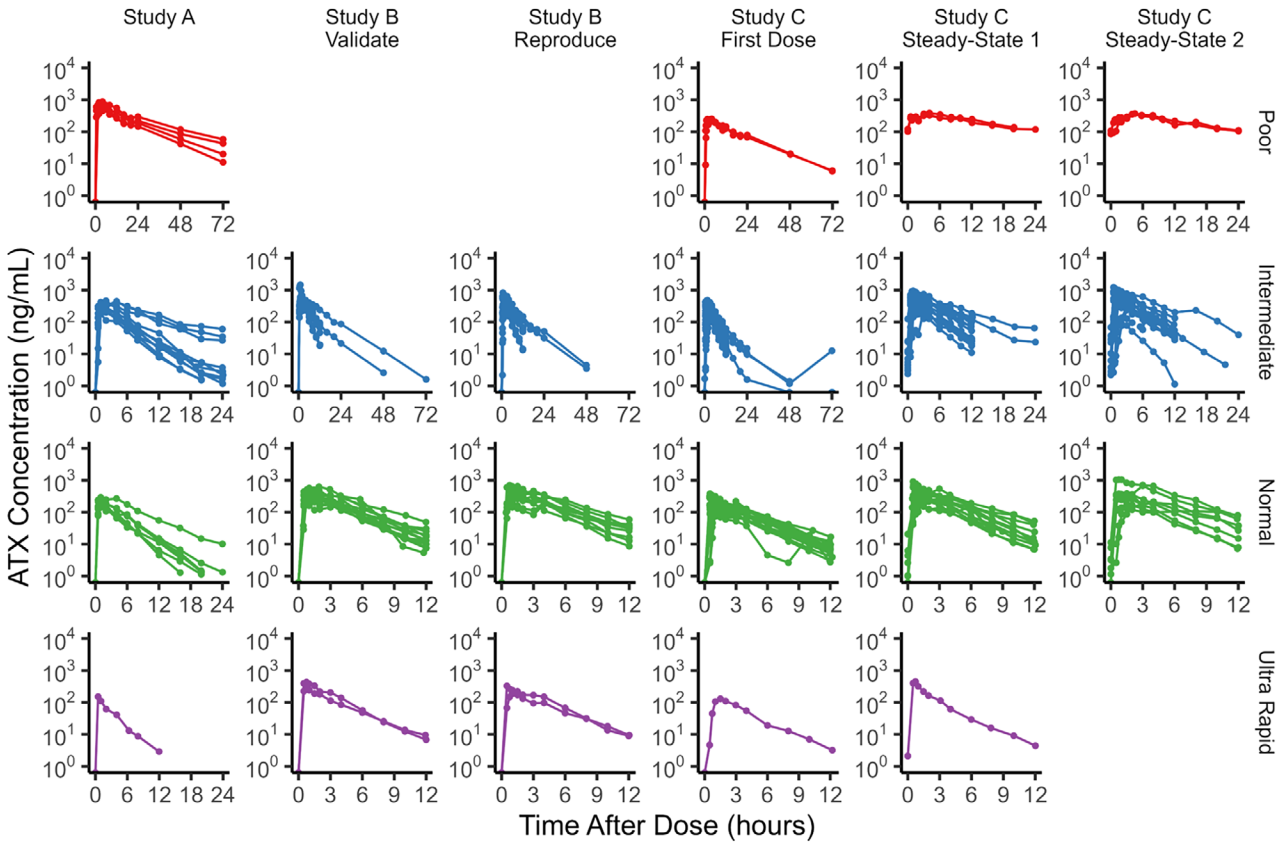

Figure 1. Individual atomoxetine plasma concentration over time for Studies A–C at different visits. Symbols represent observed data points, and lines connect individual observed data points. Color represents CYP2D6 enzyme activity phenotype. ATX, atomoxetine.

Plots of individual atomoxetine plasma concentrations are shown in Figure 1, stratified by study, occasion, and CYP2D6 phenotype. Overall, 1946 atomoxetine plasma concentration observations were used for model building. Atomoxetine absorption is unpredictably rapid or delayed after a single dose or after regular daily dosing. When using a flat weight-based dosing (Study A), the exposure of atomoxetine increases as CYP2D6 enzyme activity decreases. Of the 24 participants who completed the "model validation" session, 21 completed the "reproducibility" session. Using the internally developed models for dose selection reduced the variability in the atomoxetine exposures across the different enzyme activity groups in Study B, and the atomoxetine plasma concentrations appear reproducible after a washout. Of the 39 participants who initiated Study C, 30 participants completed the first steady-state PK session at week 6, and 22 participants completed the second steady-state PK session at week 18. Additionally, accumulation at steady state is evident for only CYP2D6 PMs at steady-state.

Table 2 shows the NCA results stratified by CYP2D6 phenotype and dosing scenario. The dose-normalized C_{max} and $AUC_{0\text{-}24h}$ decrease as CYP2D6 enzyme activity increases at both single-dose and steady-state dosing scenarios. CYP2D6 PMs show 130% and 624% higher dose-normalized C_{max} and $AUC_{0\text{-}24h}$, respectively, compared to NMs. On average, CYP2D6 PMs show over 2-h longer t_{max} compared to the other CYP2D6 phenotypes at both dosing scenarios. As expected, half-life decreased with increasing CYP2D6 enzyme activity. Table S2 shows the observed C_{max} from the NCA analysis. Steady-state atomoxetine plasma concentrations in Study C for PMs may not have been adequately represented by the internally developed model. The observed C_{max} at steady-state for PMs (362 ± 25 ng/mL) was numerically lower than the other groups (626 ± 286, 444 ± 242, 452 ng/mL for IMs, NMs, and PMs, respectively) and the target theoretical therapeutic concentration (400 ng/mL). This suggests that those participants were underdosed when selecting a dose based on the internally developed model.

Population Pharmacokinetic Modeling

Structural Model. A one-compartment distribution model with zero-order transit into a depot compartment and first-order absorption into the central compartment with first-order elimination best described the atomoxetine plasma concentration in children and adolescents. Diagnostic goodness-of-fit plots for the

Table 2. Atomoxetine NCA Results Stratified by CYP2D6 Phenotype and Dosing Scenario (Mean ± Standard Deviation). One Participant was Removed from Analysis Since Their Study Terminated Early Before Atomoxetine Concentrations Reached the Elimination Phase and Another was Removed due to Multiple Doses in One Day.

			CYP2D6 Phenotype			
Dosing Scenario	Characteristic	Overall	Poor	Intermediate	Normal	Ultra Rapid
Single Dose	Number of Individuals/Occasions	N = 106	N = 6	N = 51	N = 43	N = 6
	Dose Normalized C_{max} (ng/mL/mg)	71 ± 64	275 ± 47	79 ± 46	40 ± 18	23 ± 10
	Dose Normalized $AUC_{0\text{-}24hr}$ (ng·hr/mL/mg)	11.7 ± 6.8	21.8 ± 3.4	12.8 ± 7.5	9.5 ± 4.5	7.0 ± 4.4
	Tmax (hr)	1.72 ± 1.24	4.32 ± 0.81	1.73 ± 1.09	1.46 ± 1.09	0.92 ± 0.47
	Half Life (hr)	4.3 ± 4.7	17.3 ± 4.9	4.5 ± 4.6	2.5 ± 0.6	2.3 ± 0.4
Steady-State	Number of Individuals/Occasions	N = 51	N = 4	N = 26	N = 20	N = 1
	Dose Normalized C_{max} (ng/mL/mg)	107 ± 132	512 ± 36	92 ± 71	50 ± 24	24
	Dose Normalized $AUC_{0\text{-}24hr}$ (ng·hr/mL/mg)	16 ± 10	36 ± 2	17 ± 10	11 ± 6	11
	Tmax (hr)	1.56 ± 1.35	4.17 ± 0.24	1.36 ± 1.27	1.35 ± 1.04	0.72
	Half Life (hr)	4.2 ± 4.7	12.2 ± 1.8	3.3 ± 1.3	3.8 ± 6.3	2.2

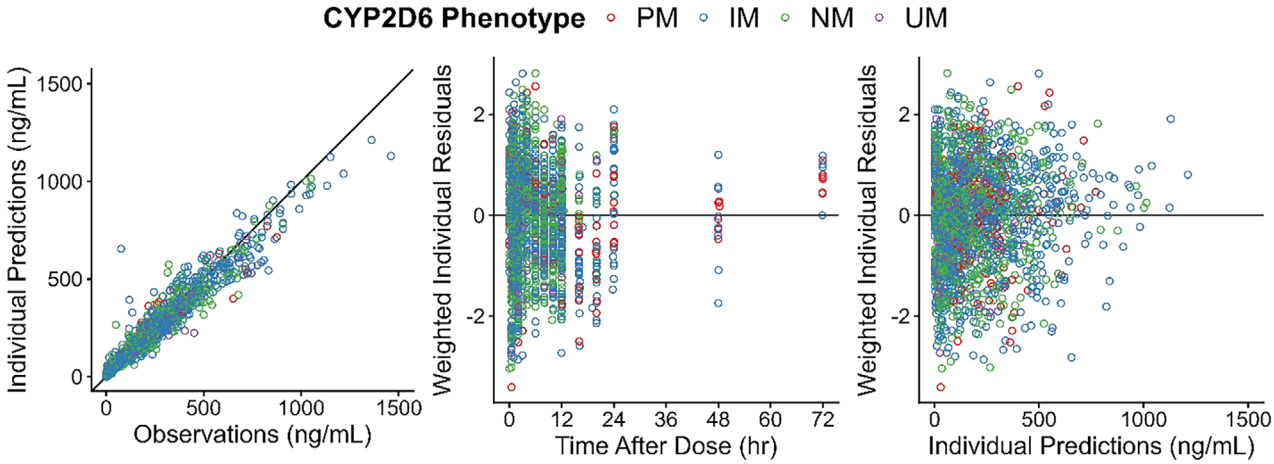

Figure 2. Goodness-of-fit plots for atomoxetine. Black lines indicate the line of identity or the zero line. Color represents CYP2D6 enzyme activity phenotype. PM, poor metabolizer; IM, intermediate metabolizer; NM, normal metabolizer; RM, rapid metabolizer; UM, ultrarapid metabolizer.

final structural model are shown in Figure 2 stratified by CYP2D6 phenotype. Observed atomoxetine plasma concentrations are adequately distributed around the line of identity on an individual level, suggesting acceptable predictability of the model. Individual weighted residuals over time and atomoxetine concentrations exhibit uniform distributions around the zero line, suggesting adequate structural and error models. Goodness-of-fit plots did not reveal systematic trends when stratifying by CYP2D6 phenotype (Figure S1) or by body weight (Figure S2), suggesting consistent model performance across these covariates. Histograms of individual parameter estimates are presented in Figure S3, showing approximately log-normal distributions for all parameters. The population parameter estimates from the structural model are shown in Table S3. The estimated zero-order duration into the depot was 0.75 h, and the estimated first-order rate constant was 27.35/h. Typical parameter estimates showed acceptable precision using 200 bootstrapped populations with a relative standard error (RSE) <11%. The estimated apparent central volume and clearance were estimated as 99.0 L and 23.4 L/h, respectively. A combination additive and proportional error model best described RUV, with estimates of 0.81 ng/mL and 21 CV%, respectively. BSV was estimated on zero-order duration, first-order rate constant, apparent volume, and apparent clearance with acceptable shrinkage (<15%).

Covariate Model. Relationships between EBEs and covariates were observed using the base structural model for actual body weight and obesity on $\eta_{Vc/F}$ and $\eta_{CL/F}$ and for CYP2D6 and CYP2C19 phenotypes on $\eta_{Vc/F}$ and $\eta_{CL/F}$ (Figure S4). A visual representation of changes in parameter variability with covariate addition is shown in Figure S5. Applying allometric scaling centered around a typical weight of

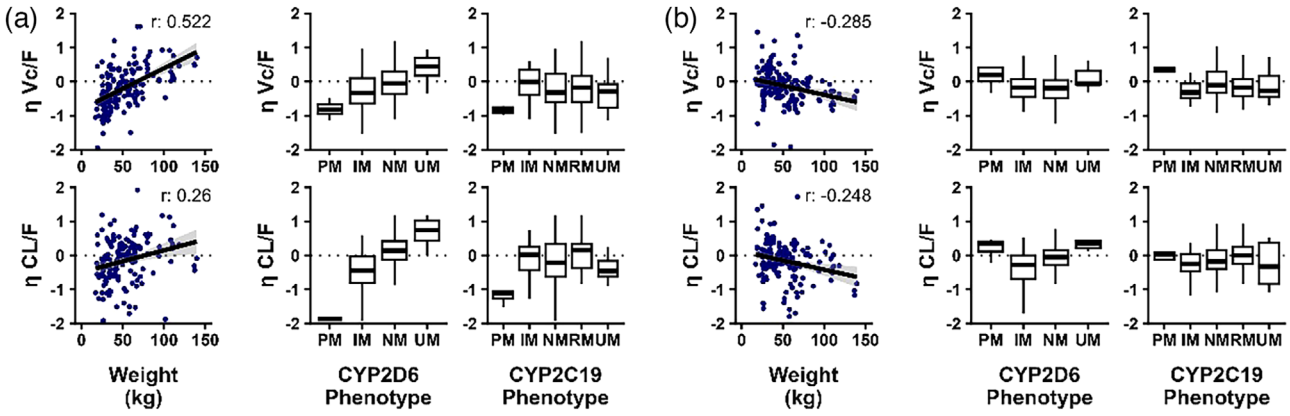

Figure 3. EBEs for apparent clearance and apparent volume from the base structural model (a) and the final covariate model (b), stratified by individual weight and metabolizer phenotypes. The dotted line represents the zero line. Pearson's correlation coefficient is displayed for weight. PM, poor metabolizer; IM, intermediate metabolizer; NM, normal metabolizer; RM, rapid metabolizer; UM, ultrarapid metabolizer.

70 kg on Vc/F (exponent: 1.0) and CL/F (exponent: 0.75) reduced the BSV of Vc/F by 9%, but did not reduce the variability in CL/F. Allometric scaling was still included on both Vc/F and CL/F due to the observed reduction in actual body weight and obesity relationships on $\eta_{Vc/F}$ and $\eta_{CL/F}$. Applying relative bioavailability of CYP2D6 PM reduced the variability of Vc/F and CL/F by 5% and 4%, respectively, and reduced the relationship of CYP2D6 phenotype on $\eta_{Vc/F}$. Due to the CYP2D6 phenotype relationship on $\eta_{CL/F}$ still being present, the effect of CYP2D6 PM on CL/F was included, reducing the variability by 9%. Relative bioavailability of CYP2D6 IM was included next, reducing the variability in Vc/F and CL/F by 2% and 3%. Due to $\eta_{CL/F}$ being relatively low for CYP2D6 IMs, the effect of CYP2D6 IM on CL/F was investigated, but did not explain the variability. Relative bioavailability or clearance effects of CYP2D6 UMs did not explain variability in Vc/F nor CL/F. Finally, the relative bioavailability of CYP2C19 PM was added, which reduced the variability in Vc/F and CL/F by 1% and 2%, respectively. Sequential addition of these covariates reduced the EBEs relationships (Figure S6) and significantly reduced the objective function value (AIC difference >2). Comparisons between the EBEs from the base structural model and the final covariate model are shown in Figure 3, demonstrating a reduction in systematic trends.

The relative bioavailabilities of CYP2D6 PMs and IMs were estimated as 3.02 and 1.33, respectively, compared to NMs, while the relative bioavailability of CYP2C19 PMs was estimated as 2.32. When stratifying by ethnicity, Asians showed relatively lower Ka, Vc/F, and CL/F but were not included as a covariate due to having only one Asian participant (with two PK visits) in the dataset. The clearance effect was estimated as −0.81% for CYP2D6 PMs. The full covariate model reduced the Vc/F BSV from 81.6% to 64.5% and reduced the CL/F BSV from 92.4% to 75.5%.

Model Qualification. Final model parameter estimates from bootstrap simulations performed 200 times are shown in Table 3. Mean parameter estimates are within the 95% confidence intervals, demonstrating the stability of the final PK model. The accuracy of the final covariate model was assessed using VPC and QPC on 1000 bootstrapped populations sampled from the original population. By non-parametrically sampling the individual/occasion instances, the relationships between parameters are inherently retained, mitigating the need to estimate and apply covariation matrices. Due to the low sample sizes of PM and UM individuals (n = 1-6) for either dosing scenario, these groups were excluded from model qualification. With limited observations in these groups, percentile estimates could become unstable and may misrepresent model performance. Excluding these groups helped preserve the interpretability of the model qualification, while these subgroups were assessed through individual fits.

Figure 4 shows a VPC plot generated by simulating atomoxetine plasma concentrations over time for 1000 populations resampled from the original population (maintaining CYP2D6 phenotype and dosing scenario sample sizes). The VPC plots show adequate matching, with observed profiles across different CYP2D6 phenotypes and at different dosing scenarios. The simulated median atomoxetine concentrations were lower than the observed median atomoxetine concentrations at earlier time points for IMs at steady-state; however, the rest of the observed percentiles fall within the 95% prediction intervals, suggesting the model captures the typical PK profile and the variability of the data reasonably well. The confidence intervals around the

Table 3. Covariate Model Parameter and Uncertainty Estimates. CI: Confidence Interval; RSE: Relative Standard Error. Covariates were Applied on Apparent Central Volume and Apparent Central Clearance using the Equations

Parameter	Description	Estimate	95% CI	RSE (%)	Shrinkage (%)
Dur	Zero-order Duration into Depot (hr)	0.75	[0.64,0.88]	7.76	
ka	First−order Absorption Rate Constant (hr^{-1})	27.35	[22.44,32.77]	10.1	
Vc/F	Apparent Central Volume (L)	175.94	[148.48,217.50]	9.46	
CL/F	Apparent Central Clearance (L/hr)	39.03	[33.90,46.33]	8.14	
$E_{CYP2D6,PM}$	Effect of CYP2D6 PM on Clearance	−0.81	[−0.84,−0.78]	1.95	
$Frel_{CYP2D6,PM}$	Relative Bioavailability of CYP2D6 PMs	3.02	[2.38,3.77]	11.67	
$Frel_{CYP2C6,IM}$	Relative Bioavailability of CYP2D6 IMs	1.33	[0.95,2.01]	20.97	
$Frel_{CYP2C19,PM}$	Relative Bioavailability of CYP2C19 PMs	2.32	[1.65,3.24]	18.27	
Between-Subject Variability (BSV)					
Ω^2_{dur}	BSV on Zero-order Duration into Depot (CV%)	127.42	[100.64,150.30]	13.79	0.00
Ω^2_{ka}	BSV on Absorption Rate Constant (CV%)	182.7	[146.09,244.82]	14.03	0.00
$\Omega^2_{Vc/F}$	BSV on Apparent Central Volume (CV%)	64.52	[45.08,76.48]	21.32	15.88
$\Omega^2_{CL/F}$	BSV on Apparent Central Clearance (CV%)	75.48	[45.82,93.55]	26.29	15.52
Residual Unexplained Variability (RUV)					
σ^2_{add}	Additive RUV (ng/mL)	0.81	[0.38,1.21]	50.78	
σ^2_{prop}	Proportional RUV (CV%)	21.39	[19.36,23.63]	10.17	
Covariate Equations					
$Vc/F_i = Vc/F_{tv} \cdot (\frac{wt_i}{70})^{1.0} \cdot (\frac{1}{Frel_{CYP2D6}}) \cdot (\frac{1}{Frel_{CYP2C19}}) \cdot e^{\eta_{Vc/F,i}}$					
$CL/F_i = CL/F_{tv} \cdot (\frac{wt_i}{10})^{0.75} \cdot (\frac{1}{Frel_{CYP2D6}}) \cdot (\frac{1}{Frel_{CYP2C19}}) \cdot (1 + E_{CYP2D6,PM}) \cdot e^{\eta_{CL/F,i}}$					

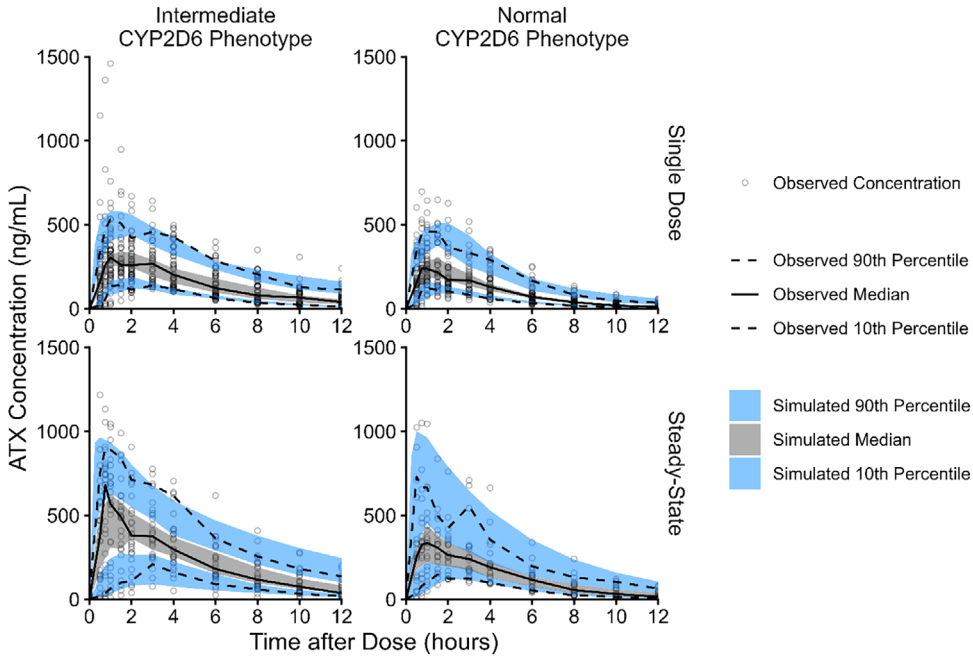

Figure 4. Visual predictive checks for atomoxetine plasma concentration over time, stratified by CYP2D6 phenotype and dosing scenario from 1000 replicated data sets resampled from the original dataset. Solid black lines show the observed median, and dashed black lines show the observed 10th and 90th percentiles of atomoxetine plasma concentration over time. The shaded regions represent the 95% confidence interval around the predicted median (gray) and 10th and 90th percentiles (blue) of atomoxetine plasma concentration over time. ATX, atomoxetine.

quantiles for NMs at steady-state were wider due to the lower number of subjects in that group (n = 20). The VPC was only analyzed up to 12 h due to some subjects not having measured concentrations beyond 12 h, leading to the observed quantiles beyond that point not being representative.

QPC analysis demonstrated overall good predictability of the atomoxetine C_{max} and $AUC_{0\text{-}24h}$ across different CYP2D6 phenotypes and dosing scenarios (Figure 5). However, the observed median C_{max} for IMs at steady-state was higher than the 95th percentile of simulated median C_{max}. The prediction error

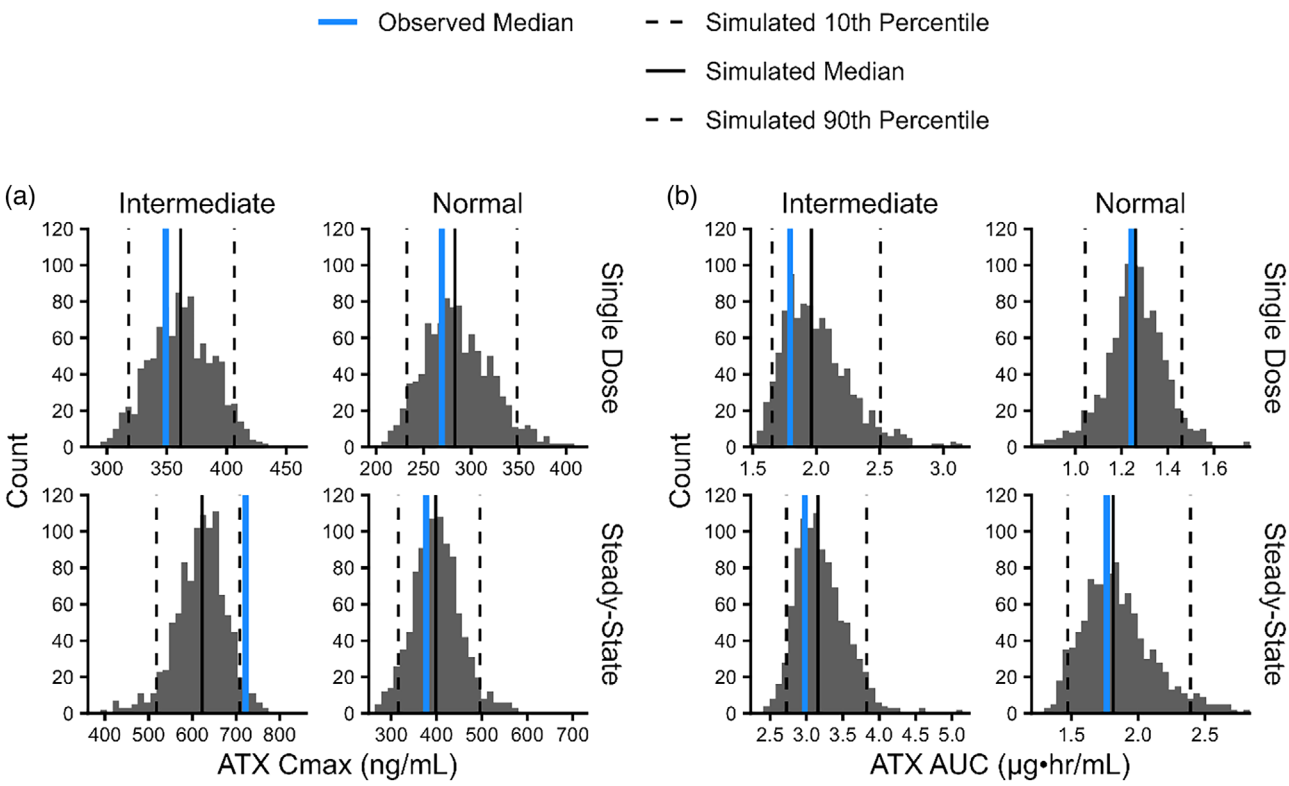

Figure 5. Qualitative predictive check for atomoxetine stratified by CYP2D6 phenotype and dosing scenario from 1000 replicated data sets resampled from the original dataset. Vertical blue lines represent the observed median exposure. The histograms show the distribution of median (a) C_{max} and (b) $AUC_{0\text{-}24h}$ of 1000 simulated datasets. Vertical black lines represent the 5th, 50th, and 95th percentiles of simulated exposure. The median percent error for C_{max} at a single dose was 3.6% (95% CI: −10.1, 18.2) and 5.1 (95% CI: −16.5, 35.1), for IMs and NMs, respectively. The median prediction error for C_{max} at steady-state was −13.8% (95% CI: −33.5, 1.0) and 5.7 (95% CI: −20.6, 39.2), for IMs and NMs, respectively. The median percent error for $AUC_{0\text{-}24h}$ at a single dose was 9.4% (95% CI: −9.9, 48.4) and 1.6 (95% CI: −21.7, 21.9), for IMs and NMs, respectively. The median percent error for $AUC_{0\text{-}24h}$ at steady-state was 6.1% (95% CI: −10.9, 33.3) and 2.8 (95% CI: −19.0, 41.6), for IMs and NMs, respectively. PMs and UM were removed from stratification due to the small sample size. ATX, atomoxetine.

for this group was −13.8% (95% CI: −33.5, 1.0), and because the 95% CI includes zero, the discrepancy is not considered statistically significant. This suggests that while the point estimate slightly underpredicts the observed value, the model's performance remains within an acceptable range of variability. Further, the range of concentrations for this group is well above the therapeutic target (400 ng/mL) and can still be reliably used to assess whether the C_{max} target is achieved. Ultimately, the final population PK model of atomoxetine captures the atomoxetine plasma profiles of this large heterogeneous population of children and adolescents.

Discussion

Currently, atomoxetine is prescribed in children and adolescents at the same initial weight-based dose regardless of CYP enzyme activity.[8] The FDA label recommends a minimum of 3 days for extensive metabolizers (CYP2D6 non-PMs) and 4 weeks for CYP2D6 PMs before titrating the dose (if no clinical response and in the absence of adverse events). More recently, a CPIC guideline was published for atomoxetine dosing based on updated CYP2D6 phenotype assignments (including the four phenotypes investigated here). The guideline recommends the same initial dose as recommended in the label, regardless of CYP2D6 phenotype; however, titration is recommended at 2 weeks for PMs and IMs (if no clinical response and in the absence of adverse events). Atomoxetine usually takes 2-4 weeks to observe the full clinical effect.[14] Additionally, it is recommended in this guideline to consider obtaining plasma concentrations and proportionally increasing the dose to achieve the proposed therapeutic target of 400 ng/mL. Providing physicians with improved tools to more precisely dose children and adolescents based on CYP enzyme activity phenotypes and other participant demographics could help participants with ADHD achieve therapeutic levels of atomoxetine faster and without the need for blood drawing. In the present study, a nonlinear mixed-effect model was developed to characterize the pharmacokinetics of atomoxetine in children and adolescents with differing levels of CYP2D6 and CYP2C19 enzyme activities.

Structural Model

The structural population PK model presented here displayed good predictive performance. The estimated typical values for Vc/F (98.96 L) and CL/F (23.45 L/h) are both similar to the previously reported distribution parameters.[4] This apparent volume is similar to the label-reported volume from intravenous administration: 110.25 L (based on a 0.63 absolute bioavailability for a normal metabolizer).[8] The zero-order duration into the depot was estimated to be 0.75 h, which aligns with the maximum concentration in NMs occurring approximately 1.3 h after the dose, since the atomoxetine in the depot would continue entering the systemic circulation from the depot. The first-order rate constant of atomoxetine entering the systemic circulation was estimated to be 27/h. The parameter distributions for zero-order duration and first-order rate constant show a large portion at the bounds. This was due to the limits set for each parameter since the instances of rapid absorption had near zero hour duration and extremely high first-order absorption. Simulations demonstrated that first-order rate constants above 50/h had minimal visual differences in atomoxetine concentrations. When the limits were not placed on these parameters, the BSV inflated. The BSV for these parameters was still relatively large (127% CV and 182% CV for zero-order duration and first-order rate constant, respectively), further emphasizing the high variability in atomoxetine absorption between subjects and occasions. The precision of the final model parameter estimates was assessed using 200 bootstrapped populations sampled from the individual parameter distributions. The precision was acceptable with a <28% RSE except for the additive RUV, which showed a higher RSE (>50%) due to one subject with an estimated 150 ng/mL additive error.

The data from Study A have been previously reported by Brown et al[3] and Cheng et al[4]; the latter group proposed a model consisting of four transit compartments for absorption and two distribution compartments for atomoxetine with linear elimination to multiple metabolite pathways terminating in urine compartments.[4] While Cheng et al model involved multiple metabolite pathways to better understand contributions of competing CYP enzyme activity, the present PK model focuses on parent atomoxetine concentrations due to its intended clinical application. The high genetic polymorphism of CYP enzymes causes the systemic exposure of atomoxetine in children and adolescents to be highly variable.[4,15] CYP2D6 is primarily responsible for converting atomoxetine into the equipotent 4-hydroxyatomoxetine, with this pathway accounting for approximately 95% of the parent atomoxetine's metabolism.[2] Despite this metabolic pathway being the most abundant, the measured concentration of 4-hydroxyatomoxetine in plasma following oral doses of atomoxetine is low (~1% of the concentration of atomoxetine) due to the rapid conjugation to the inactive 4-hydroxyatomoxetine glucuronide.[2] CYP2C19 is another important enzyme for atomoxetine elimination, responsible for the conversion to N-desmethylatomoxetine followed by conversion to N-desmethyl-4-hydroxyatomoxetine, both of which are inactive. This pathway dominates when CYP2D6 activity is compromised (i.e., CYP2D6 PMs).[4,16] However, due to this low proportion of the active metabolite present in the systemic circulation compared to parent atomoxetine, metabolite pathways were not analyzed in the present PK model.

Based on the observed data from combining all three studies, atomoxetine exhibits one-compartment behavior as evidenced by the absence of a distribution phase (single phase linear decline in plasma concentrations following C_{max}). A single-compartment model for atomoxetine was presently used based on the observed data. While Study A data displayed primarily rapid absorption of atomoxetine, the additional studies demonstrated high variability in atomoxetine absorption between occasions within individuals. This led to the necessity of using a two-stage approach when combining the three studies.

Two-Stage Methodology

The present population PK model includes data from three different studies, including single-dose events and dosing at steady-state, which has not been modeled previously. While initially exploring the combined data, a one-stage analysis was performed with unsuccessful model convergence. Bias in the individual predictions was evident, particularly at lower concentration levels, where the model consistently overpredicted concentrations (data not shown). Through exploratory data analysis, it was determined that some atomoxetine profiles exhibit rapid absorption while others exhibited a delayed absorption. Discrepancies were also observed within the same subject at different occasions without a clear relationship between occasion and individual. Example cases that demonstrate this phenomenon are presented in Figure S7. Additionally, a similarly inconsistent second peak was observed for multiple subjects at approximately 5 h after the dose. There were also discrepancies present for dosing and resulting PK profiles. For instance, U01 and U02 showed lower C_{max} despite increases in their dose between occasions, whereas U12 exhibited C_{max} of approximately 200, 600, and 400 ng/mL despite similar doses between occasions. Between-occasion variability (BOV) on absorption parameters was included along with BSV in the one-stage analysis to attempt to explain these differences with unsuccessful model convergence. An extensive exploratory analysis of these patterns was performed to potentially predict the absorption rate or

presence of a secondary peak. Comparisons between absorption rate or presence of a secondary peak to time of food intake relative to dose administration, nutritional intake profiles, dose level, CYP2D6 phenotype, body weight, and other participant demographics (data not shown) were assessed. No significant trends were observed demonstrating the unpredictability of the absorption in atomoxetine pharmacokinetics in children and adolescents.

For successful model convergence and to improve model predictability, each participant/occasion instance was treated as a separate individual, and the population PK model was developed using a two-stage approach. Treating each participant/occasion as an individual combines the BSV and BOV for population-level parameters. Due to the high variability in atomoxetine absorption between subjects and occasions, the BOV could not be reliably estimated using a one-stage approach. For a two-stage approach, individual profiles are modeled, followed by a summary of the individual PK parameter estimates to obtain population-level estimates. Whereas in a one-stage approach, all participants are modeled simultaneously to obtain population-level estimates, and random effects are used to assess BSV.[17] The PK data used presently are rich profiles for a majority of the participants/occasions (one subject terminated the study early). This justifies the use of the two-stage approach since it does not need other profiles to inform the individual profiles, which would be necessary for sparse data. One potential limitation of a two-stage approach is the bias in variability estimates.[18,19] Two-stage approaches tend to overestimate BSV because the individual estimates are treated as "true" values, ignoring the uncertainty in those estimates. Additionally, the covariate analysis is not incorporated directly into the PK model; instead, it is performed *post hoc* on potentially complex, irregular distributions of individual parameter estimates. This approach is susceptible to attenuation bias or false relationships.[20] These limitations were considered acceptable for the current analysis due to low shrinkage (<16%), indicating that the EBEs reliably reflect true individual variability. Ultimately, the one-stage approach was deemed unsuitable for analyzing the highly variable and complex patterns of atomoxetine absorption observed in the present dataset. Instead, a two-stage approach was used to characterize the pharmacokinetics of atomoxetine in children and adolescents.

Impact of Covariates

Similar to the Cheng et al model,[4] adding allometric scaling for actual body weight on apparent clearance and apparent volume, CYP2D6 phenotype relative bioavailability compared to NMs on apparent clearance and apparent volume, and CYP2D6 phenotype clearance effects as covariates sufficiently explained BSV in the atomoxetine PK. Due to atomoxetine being administered orally, only the apparent volume and apparent clearance can be estimated. Adding allometric scaling for actual body weight using conventional exponents (1.0 for volume and 0.75 for clearance) centered around a 70-kg typical adult adequately explained the BSV in apparent volume and clearance by body weight and obesity. In the present model, allometric scaling was centered on the typical adult weight, despite the PK data being solely from children and adolescents (~55 kg), to have the model be adaptable and comparable. The use of conventional allometric scaling exponents in the present model, as applied in the Cheng et al model,[4] is mechanistically based on the metabolic differences across body weights.[21] Centering on typical adult weights allows for comparability of parameter estimates between models regardless of population. As shown in Figure 3, trends in apparent volume were reduced to a greater extent than those in apparent clearance following inclusion of allometric scaling, likely due to the larger allometric exponent and its greater influence on apparent volume. However, the spread in apparent clearance and apparent volume around zero was improved when incorporating allometric scaling.

Bioavailability or clearance effects are apparent when comparing dose-normalized $AUC_{0\text{-}24h}$ by CYP2D6 phenotypes (Table 2). While IMs, NMs, and UMs show similar $AUC_{0\text{-}24h}$, PMs have almost ninefold higher $AUC_{0\text{-}24h}$. The $\eta_{Vc/F}$ over CYP enzyme phenotypes exhibited a trend which can be attributed to the relative bioavailability, since the enzyme phenotype should not have an effect on atomoxetine distribution volume. Relative bioavailability adjustments were only included for CYP2D6 PMs and IMs, as incorporating UMs did not adequately explain the variability in atomoxetine PK. Compared to NMs (fixed at 1.0), the estimated relative bioavailability was 3.02 for PMs and 1.33 for IMs, indicating approximately 3-fold and 1.3-fold higher bioavailability, respectively. This suggests the presence of extensive pre-systemic clearance for atomoxetine. This is corroborated by Cheng et al, as they showed that PMs and IMs have a higher relative bioavailability compared to NMs and UMs, which have a similar relative bioavailability.[4] The relative bioavailability differences between CYP2D6 phenotypes are much higher than previously reported,[4] likely due to additional participants improving phenotype representation, revealing real exposure differences that were previously underestimated. In Study A, participants were dosed based on body weight, whereas in the additional studies used in the present analysis, model-based dosing incorporating CYP2D6 phenotype was utilized to achieve a target

peak concentration of 400 ng/mL. The previously estimated relative bioavailability effects could have been masked by the clearance differences between participants when receiving the same body weight-based dose. When exposures were adequately matched between CYP2D6 phenotypes to account for clearance differences, the observed differences in exposure are more likely due to the bioavailability.

After adding the relative bioavailability of CYP2D6 PMs as a covariate, the clearance effects of CYP2D6 PMs were still evident, leading to the addition of CYP2D6 PMs clearance effects. This effect was estimated as an 81% reduction in clearance for CYP2D6 PMs compared to CYP2D6 NMs. Clearance effects of IMs and UMs did not adequately explain variability in the current analysis, whereas the Cheng et al model[4] estimated clearance effects for PMs and IMs and a slight clearance effect from UMs compared to NMs. The clearance effects could have masked the relative bioavailability effects, as stated previously. Prioritizing relative bioavailability before clearance effects was justified by the mirrored relationships observed in $\eta_{Vc/F}$ and $\eta_{CL/F}$ on CYP2D6 phenotype (Figure S4). Further, the additional participants in the combined dataset may be more informative of clearance and relative bioavailability effects.

In addition to these covariates, our study determined that adding relative bioavailability of CYP2C19 PMs statistically improved model fits (P value $<.05$ using likelihood ratio test) and better centered apparent volume and $\eta_{CL/F}$ around zero (Figure S6). The estimated relative bioavailability of CYP2C19 PMs was 2.32 compared to CYP2C19 NMs (fixed at 1.0), indicating approximately 2.3-fold higher bioavailability. While this only involved two individuals (four total dosing occasions) and should be interpreted with caution, the covariate effect aligns with physiological expectations, and an approximate twofold difference in relative bioavailability is clinically meaningful. These two participants were CYP2D6 IMs, suggesting that more atomoxetine is available for the N-desmethylatomoxetine pathway, with the potential to be affected by CYP2C19 genotype/activity, with CYP2C19 PMs producing higher bioavailability. Additionally, the EBEs showed substantial and consistent differences in $\eta_{Vc/F}$ and $\eta_{CL/F}$ for these CYP2C19 PMs, indicating that CYP2C19 PMs may not receive adequate dosing if not accounted for. No relationships in absorption parameter EBEs were observed for the potential covariates tested, further illustrating the unexplained variability in atomoxetine absorption.

Future Directions

A key limitation of this analysis is the small sample size for CYP2D6 PMs and CYP2D6 UMs, which restricted model qualification in these subpopulations. Similarly, the number of CYP2C19 PMs and Asian participants was small. While the linear PK of atomoxetine reduces the risk associated with extrapolating to steady-state in these groups, further studies including more participants from these subpopulations would strengthen confidence in phenotype-based dose recommendations. Additionally, incorporating genetic ancestry in future studies, rather than relying on self-identified ethnicity as in the present study, could provide additional model-relevant information.

Precision medicine has the potential to improve treatment outcomes by optimizing dosing to achieve efficacy while minimizing toxicity. Given the high variability in atomoxetine exposures across CYP phenotypes, a uniform dosing approach is not optimal. The current qualified model enables simulation of atomoxetine exposures based on participant demographics and can support the identification of adequate typical target doses likely to achieve therapeutic levels. A clinical support tool could be developed using this model that could be used to provide participants with better dose schedules to ensure they achieve therapeutic levels. This support tool could incorporate participant characteristics, including body weight, first dose exposure checks, known CYP enzyme phenotypes, and knowledge of CYP enzyme inducer/inhibitor, to predict expected PK profiles, expected exposure metrics, potential initial and target doses.

More exciting is the potential for model-informed dosing and control of systemic exposure to identify patients who are inherently non-responsive to atomoxetine (e.g., unlikely to respond to atomoxetine regardless of the systemic exposure achieved), leading to future investigation of the factors contributing to the non-response phenotype. The ability to predict patients who will, or will not, respond to atomoxetine (or any medication) represents an additional step toward true precision therapeutics.

Conclusions

A population PK model was developed to describe single-dose and steady-state atomoxetine exposures in children and adolescents across the spectrum of CYP2D6 and CYP2C19 activities. Significant covariate effects were observed for actual body weight, CYP2D6 and CYP2C19 on relative bioavailability and CYP2D6 on clearance. The application of the developed model to individualize dosing and reduce variability in the dose-exposure relationship has considerable potential to improve patient outcomes by reducing the risk of treatment failure due to inadequate exposure.

Conflicts of Interest

The authors declare no conflicts of interest.

Funding

Data for Study A were supported by grant 1R01HD058556, while Studies B and C were supported by grant 1P50HD090258, both from the Eunice Kennedy Shriver National Institute of Child Health and Human Development.

Data Availability Statement

The data that support the findings of this study are available from the corresponding author upon reasonable request.

References

1. Sauer JM, Ring BJ, Witcher JW. Clinical Pharmacokinetics of Atomoxetine. *Clin Pharmacokinet*. 2005;44(6):571-590. doi:10.2165/00003088-200544060-00002
2. MacKenzie KR, Zhao M, Barzi M, et al. Metabolic profiling of norepinephrine reuptake inhibitor atomoxetine. *Eur J Pharm Sci Off J Eur Fed Pharm Sci*. 2020;153:105488. doi:10.1016/j.ejps.2020.105488
3. Brown JT, Abdel-Rahman SM, van Haandel L, Gaedigk A, Lin YS, Leeder JS. Single dose, CYP2D6 genotype-stratified pharmacokinetic study of atomoxetine in children with ADHD. *Clin Pharmacol Ther*. 2016;99(6):642-650. doi:10.1002/cpt.319
4. Cheng S, Al-Kofahi M, Leeder JS, Brown JT. Population Pharmacokinetic Analysis of Atomoxetine and its Metabolites in Children and Adolescents with Attention-Deficit/Hyperactivity Disorder. *Clin Pharmacol Ther.* 2024;115(5):1033-1043. doi:10.1002/cpt.3155
5. Newcorn JH, Sutton VK, Weiss MD, Sumner CR. Clinical Responses to Atomoxetine in Attention-Deficit/Hyperactivity Disorder: The Integrated Data Exploratory Analysis (IDEA) Study. *J Am Acad Child Adolesc Psychiatry*. 2009;48(5):511-518. doi:10.1097/CHI.0b013e31819c55b2
6. Cascade EF, Kalali AH, Feifel D. STRATTERA: Ups, Downs, and Emerging Uses. *Psychiatry Edgmont*. 2007;4(4):23-25. Accessed August 28, 2024. https://www.ncbi.nlm.nih.gov/pmc/articles/PMC2921235/
7. ter Laak MA, Temmink AH, Koeken A, van 't Veer NE, van Hattum PRM, Cobbaert CM. Recognition of impaired atomoxetine metabolism because of low CYP2D6 activity. *Pediatr Neurol*. 2010;43(3):159-162. doi:10.1016/j.pediatrneurol.2010.04.004
8. Strattera (atomoxetine hydrochloride) CAPSULES for Oral Use. Prescribing information. Eli Lilly, 2002. Accessed August 14, 2024. https://www.accessdata.fda.gov/drugsatfda_docs/label/2011/021411s035lbl.pdf
9. de Leon J. The Crucial Role of the Therapeutic Window in Understanding the Clinical Relevance of the Poor Versus the Ultrarapid Metabolizer Phenotypes in Subjects Taking Drugs Metabolized by CYP2D6 or CYP2C19. *J Clin Psychopharmacol*. 2007;27(3):241. doi:10.1097/JCP.0b013e318058244d
10. de Leon J. Translating Pharmacogenetics to Clinical Practice: Do Cytochrome P450 2D6 Ultrarapid Metabolizers Need Higher Atomoxetine Doses? *J Am Acad Child Adolesc Psychiatry*. 2015;54(7):532-534. doi:10.1016/j.jaac.2015.04.003
11. Children's Mercy Hospital Kansas City. Atomoxetine PBPK-PD Clinical Study. identifier: NCT03154359. Updated August 8, 2023. Accessed August 14, 2024. https://clinicaltrials.gov/study/NCT03154359?cond=ADHD&intr=atomoxetine&page=1&rank=19
12. Gaedigk A, Simon S, Pearce R, Bradford L, Kennedy M, Leeder J. The CYP2D6 Activity Score: Translating Genotype Information into a Qualitative Measure of Phenotype. *Clin Pharmacol Ther*. 2008;83(2):234-242. doi:10.1038/sj.clpt.6100406
13. Brown JT, Bishop JR, Sangkuhl K, et al. Clinical Pharmacogenetics Implementation Consortium (CPIC) Guideline for CYP2D6 Genotype and Atomoxetine Therapy. *Clin Pharmacol Ther*. 2019;106(1):94-102. doi:10.1002/cpt.1409
14. Savill NC, Buitelaar JK, Anand E, et al. The efficacy of atomoxetine for the treatment of children and adolescents with attentiondeficit/hyperactivity disorder: a comprehensive review of over a decade of clinical research. *CNS Drugs*. 2015;29(2):131-151. doi:10.1007/s40263-014-0224-9
15. Michelson D, Read HA, Ruff DD, Witcher J, Zhang S, McCRACKEN J. CYP2D6 and Clinical Response to Atomoxetine in Children and Adolescents With ADHD. *J Am Acad Child Adolesc Psychiatry*. 2007;46(2):242-251. doi:10.1097/01.chi.0000246056.83791.b6
16. Cheng S, Flora DR, Rettie AE, Brundage RC, Tracy TS. Pharmacokinetic Modeling of Warfarin II – Model-Based Analysis of Warfarin Metabolites after Warfarin Administered Either Alone or Together with Fluconazole or Rifampin. *Drug Metab Dispos*. 2022;50(9):1302-1311. doi:10.1124/dmd.122.000877
17. Mould D, Upton R. Basic Concepts in Population Modeling, Simulation, and Model-Based Drug Development. *CPT Pharmacomet Syst Pharmacol*. 2012;1(9):6. doi:10.1038/psp.2012.4
18. Proost JH, Schiere S, Eleveld DJ, Wierda JMKH. Simultaneous versus sequential pharmacokinetic-pharmacodynamic population analysis using an iterative two-stage Bayesian technique. *Biopharm Drug Dispos*. 2007;28(8):455-473. doi:10.1002/bdd.575
19. Ette EI, Williams PJ. Population Pharmacokinetics II: Estimation Methods. *Ann Pharmacother*. 2004;38(11):1907-1915. doi:10.1345/aph.1E259
20. Savic RM, Karlsson MO. Importance of Shrinkage in Empirical Bayes Estimates for Diagnostics: Problems and Solutions. *AAPS J*. 2009;11(3):558-569. doi:10.1208/s12248-009-9133-0
21. Peters RH. *The Ecological Implications of Body Size*. Cambridge University Press; 1983. doi:10.1017/CBO9780511608551

Supplemental Information

Additional supplemental information can be found by clicking the Supplements link in the PDF toolbar or the Supplemental Information section at the end of web-based version of this article.